Letter

Physical Orphaning versus Chemical Instability: Is Dendritic Electrodeposition of Li Fatal?

Jingxu Zheng, Tian Tang, Qing Zhao, Xiaotun Liu, Yue Deng, and Lynden A. Archer

ACS Energy Lett., **Just Accepted Manuscript** • DOI: 10.1021/acsenergylett.9b00750 • Publication Date (Web): 16 May 2019

Physical Orphaning versus Chemical Instability: Is Dendritic Electrodeposition of Li Fatal?

Jingxu (Kent) Zheng[1], Tian Tang[1], Qing Zhao[2], Xiaotun Liu[2], Yue Deng[1], Lynden A. Archer[2*]

1. Department of Materials Science and Engineering, Cornell University, Ithaca, NY, 14853, USA.

2. Robert Frederick Smith School of Chemical and Biomolecular Engineering, Cornell University, Ithaca, NY, 14853, USA.

* Corresponding author: laa25@cornell.edu

Abstract: The dendritic electrodeposition of lithium, leading to physical orphaning and chemical instability, is considered responsible for the poor reversibility and premature failure of electrochemical cells that utilize Li metal anodes. Herein we critically assess the roles of physical orphaning and chemical instability of electrodeposited Li on electrode reversibility using planar and non-planar electrode architectures. The non-planar electrodes allow the morphology of electrodeposited Li to be interrogated in detail and in the absence of complications associated with cell stacking pressure. We find that physical orphaning is a key determinant of the poor reversibility of Li. We report further that fiber-like, dendritic electrodeposition is an intrinsic characteristic of Li —irrespective of the electrolyte solvent chemistry. With guaranteed electronic access to prevent physical loss, we finally show that a Li metal electrode exhibits high levels of reversibility (99.4% CE), even when the metal electrodeposits are in obvious, dendritic morphologies. We take advantage of these findings to create high-loading (7 mAh/cm^2) Li||LFP full cells with nearly unity N:P ratio and demonstrate that these cells exhibit good reversibility.

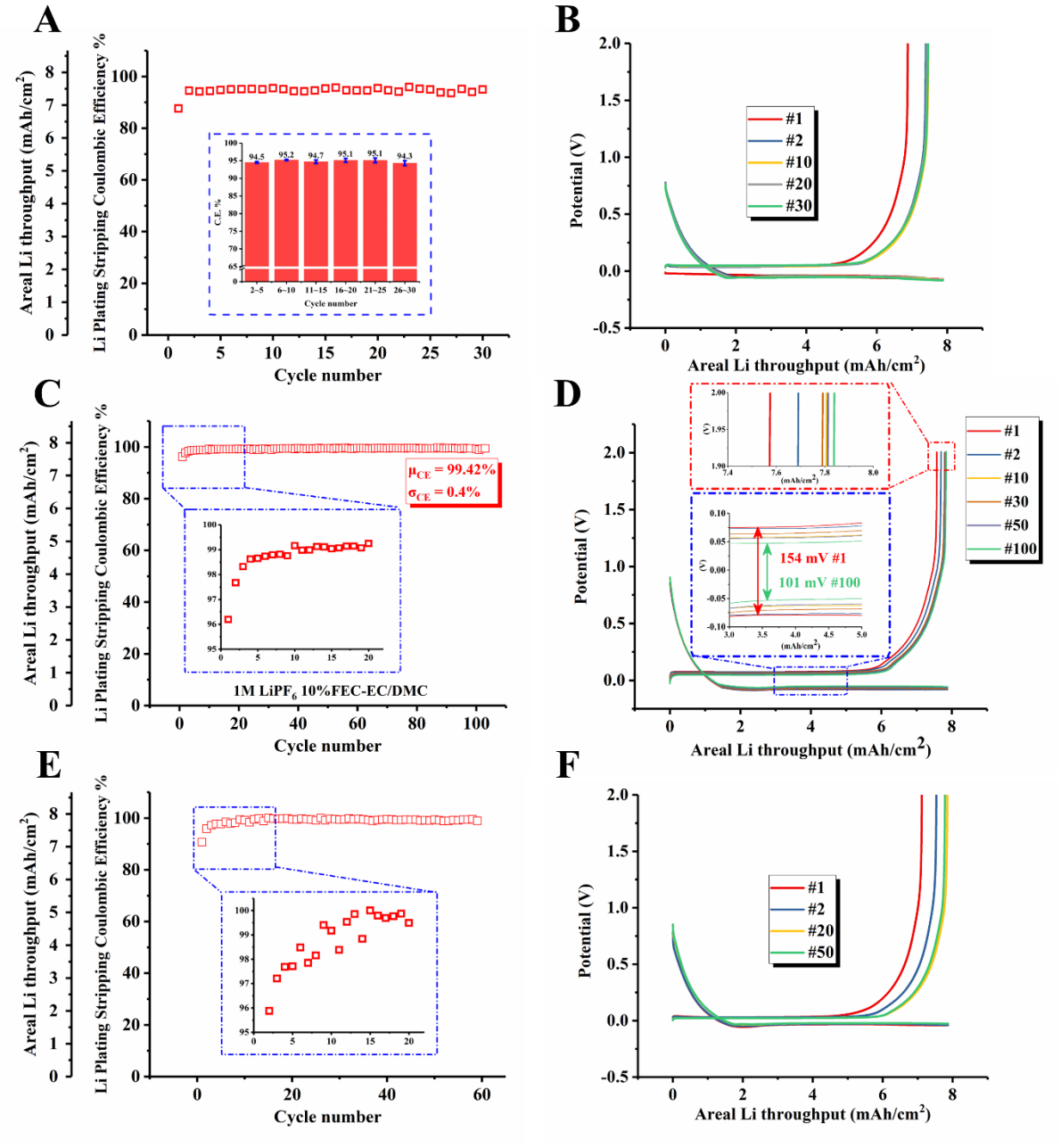

Figure 1. Li plating/stripping using a non-planar electrode. Li plating/stripping Coulombic efficiency and corresponding voltage profile in (a)(b)1M $LiPF_6$ in EC/DMC, (c)(d) 1M $LiPF_6$ in 10w%FEC-EC/DMC and (e)(f) 1M LiTFSI + 0.5% $LiNO_3$ in DOL/DME.

Main text begins:

The development of electrochemical cells based on lithium redox chemistry has witnessed a back-tracing route over the past 40 years. Although the current landscape of commercial batteries is dominated by cell chemistries in which Li is maintained in ionic form at all stages of battery cycling, these Li-ion batteries (LIBs) cannot meet emerging demands for energy-dense, cost-effective, and stable long-term electrical energy storage. This has led to a recent renewal of efforts to develop electrochemical cells in which Li is stored in reduced form in the battery anode [1] The advantages of a Lithium metal anode is on the one hand obvious — the specific capacity of Li metal (3860 mAh/g; 2061 mAh/cm^3) is high and the redox potential of Li+/Li is fully 200-300 mV lower than LiC_6 used in LIBs [1, 2]. On the other hand, Li is a highly reactive metal and can potentially fail as a result of uncontrolled chemical, morphological, and hydrodynamic processes during battery recharge [3].

The revival of interest in Li metal has produced a growing body of work in which strategies of increasing sophistication and effectiveness are employed to redesign the cell components, including the electrolyte, to mitigate the underlying instabilities. To achieve high Li plating/stripping Coulombic efficiency (CE), innovations on the solid-electrolyte interphase (SEI)[4-6], electrolyte[7-10], electrode architecture[11-14] and other cell components[15, 16] have been demonstrated. In contrast to the oftentimes highlighted overall high CE achieved in these studies, which in most literatures is contended to be positively correlated with "nondendritic" electrodeposition of Li, little research has been performed to understand the respective roles of the chemical and physical orphaning components of the total lithium loss that are the principal determinants of the overall CE. Consequently, the fundamental correlation between dendritic

deposition and Coulombic inefficiency (CI = 1 - CE) of Li anodes remain poorly understood. Notwithstanding the significant volume of recent work and with few exceptions [4, 17], the consensus in the field today is that to compensate for the too rapid loss of electrochemically active Li and consequent high Li plating/stripping CI, a large excess of Li is necessary to sustain LMB cycle life. This makes the true energy density achievable with emerging LMB technology less competitive, in comparison to what is already available commercially in LIBs [2, 18].

While the event that initiates the cascade of instabilities that produce unacceptably high CI in LMBs is still under active study [19-21], suppression of mossy/dendritic deposition during recharge is considered a requirement for progress towards practical LMBs. The present study critically assesses this requirement using planar and non-planar electrodes that allow the morphology of Li to be interrogated in detail. Significantly, we find that with guaranteed electronic access that prevents physical loss of active Li (orphaning, SI 1; also called "dead" Li issue [22-24]), a Li metal electrode can manifest high levels of reversibility, even when the metal electrodeposits exhibit obvious, dendritic morphologies. We show further that electrodes that reduce orphaning are as effective as electrolyte design for achieving high levels of reversibility. As a first step towards practical LMBs, we show that high-capacity (7~8 mAh/cm^2) Li||$LiFePO_4$ (LFP) cells with low anode to cathode capacity ratios (N/P = 1:1) can be reversibly cycled in aprotic carbonate liquid electrolytes.

The main results of the study are summarized in Figure 1 where we report the CE and voltage profiles for Li plating and stripping in various electrolytes. A non-planar carbon-cloth electrode is used for the experiments to facilitate complementary interrogation of the electrodeposit

morphology. Fig. 1A and 1B report results for a standard 1M $LiPF_6$ ethylene carbonate/dimethyl carbonate (EC/DMC) electrolyte. The high CE values (94.6% nominal CE and 93.5% real CE after subtracting the intercalation capacity (1.2 mAh/cm^2, SI 2)) and low overpotentials are substantially higher than typical (CE ~ 80% at 0.4~1 mAh/cm^2) for this electrolyte chemistry. [3, 25] The low CE for EC/DMC is thought to reflect intrinsic parasitic chemical degradation of the electrolyte and fragility of the interphases formed. As we have made no effort to address either failure mechanism, the high CE values reported in Fig. 1 clearly contest this explanation.

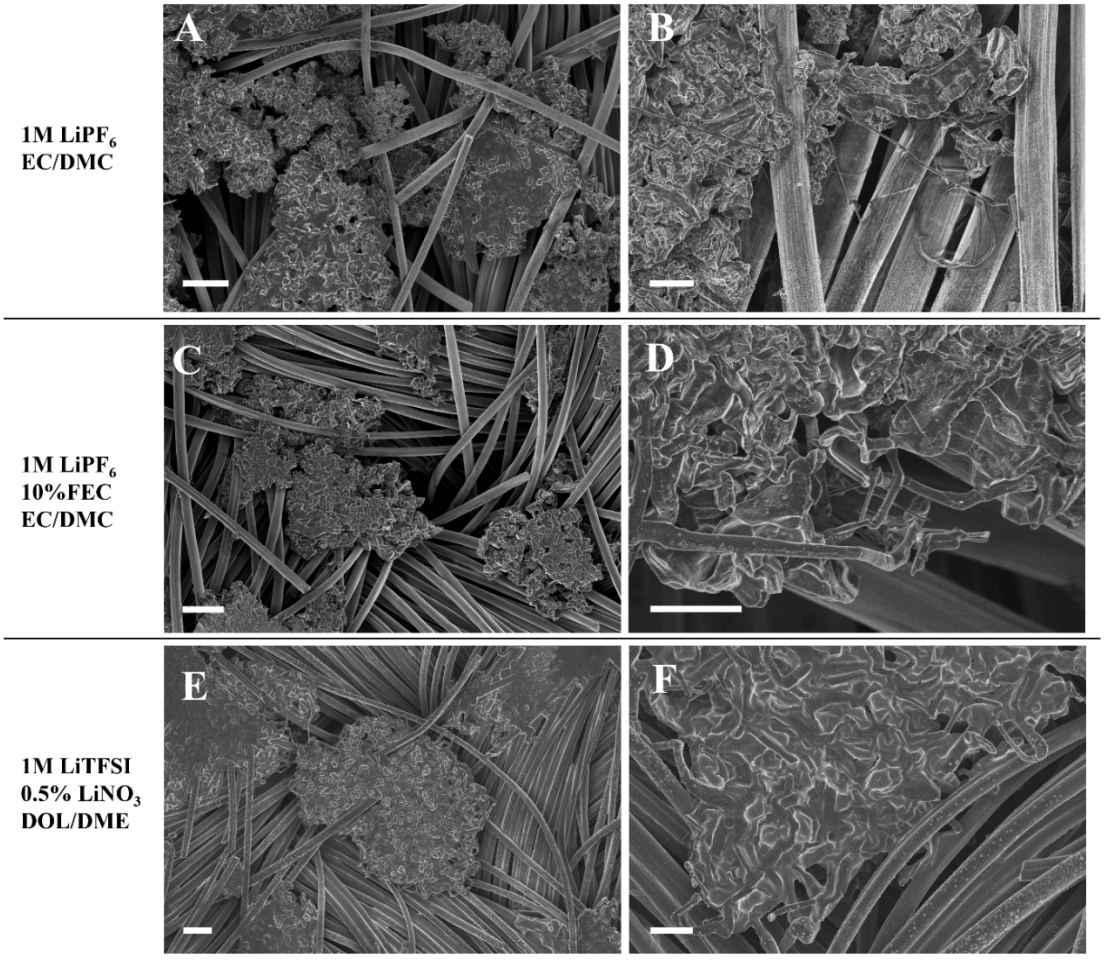

Figure 2. Li deposition morphology in a non-planar electrode. SEM images of Li deposits in (a)(b)1M $LiPF_6$ in EC/DMC, (c)(d) 1M $LiPF_6$ in 10w%FEC-EC/DMC and (e)(f) 1M LiTFSI + 0.5% $LiNO_3$ in DOL/DME. Scale bars: left (a,c,e) 40 μm; right (b,d,f) 10 μm.

Fig. 2A and 2B, report the corresponding morphology of Li deposits, which can be compared with those in SI 3 for Li on a planar Cu foil, with a Celgard 3501 separator. Both sets of results show that the deposits are composed of loosely coordinated fibrillar, thread-like structures of the order of 1 μm in diameter. We note, however, that for the same Li electrodeposit capacity (8 mAh/cm^2), the total exposed surface area of Li is significantly higher in the non-planar electrode than for the planar case. Again, this is opposite to what we observe, which appears to conclusively rule-out the chemical instability hypothesis for the low CE reported in the 1M $LiPF_6$ EC/DMC electrolyte.

Fig. 1C and 1D report CE values and voltage profiles for Li stripping/plating experiments conducted in a 1M $LiPF_6$ EC/DMC containing 10%FEC. This electrolyte composition is now widely recognized for its ability to enhance Li reversibility [26]. The FEC additive has been reported to breakdown at the Li anode to form a LiF-rich layer, which is thermodynamically stable in contact with Li and hypothesized to protect the electrolyte from continuous parasitic reactions, without compromising interfacial ion transport [25, 26]. The CE values are initially comparable to those measured in the EC/DMC system, but gradually (see inset to Fig. 1C) rise to higher values (nominal CE: 99.4% and real CE: 99.3%). Additionally, even at high Li stripping/plating capacities of 8 mAh/cm^2, the high CE values are preserved in extended cycling. The corresponding electrodeposit morphologies are reported in Fig. 2C and 2D; and SI 3 for a planar Cu electrode. The results in Figs. 2A and 2C reveal that the FEC additive has little, if any, effect on the morphology of Li deposits and there is no noticeable change in fiber diameter (SI 4). Analysis of the corresponding Li morphologies for the planar electrodes (SI 3) lead to a similar conclusion. As

a final example, we investigated Li deposition in an ether-based, 1M LiTFSI DOL/DME, electrolyte containing 0.5 wt% $LiNO_3$. Compared with carbonates, ether-based electrolytes can undergo ring-opening anionic or cationic polymerization at a Li anode [14] to form a protective polymeric coating. The results in Fig. 1E and 1F show that the initial CE is comparable to the 1M $LiPF_6$ EC/DMC, but steadily rises to high values (nominal CE: 99.4% and real CE: 99.3%). Again, the electrodeposit morphologies (Fig. 2E and 2F) show hardly perceptible differences from those reported in the other two electrolytes. And, remarkably, the morphology of the electrodeposits on the planar electrode (SI 3) are more obviously fibrous and dendritic.

On the basis of these observations, we conclude that it is possible to sustain stable, high-CE cycling of Li even when the deposition is fiber-like or dendritic. We hypothesize further that factors other than the electrolyte chemistry or electrodeposit morphology are dominantly responsible for the high CE measured for non-planar electrodes.

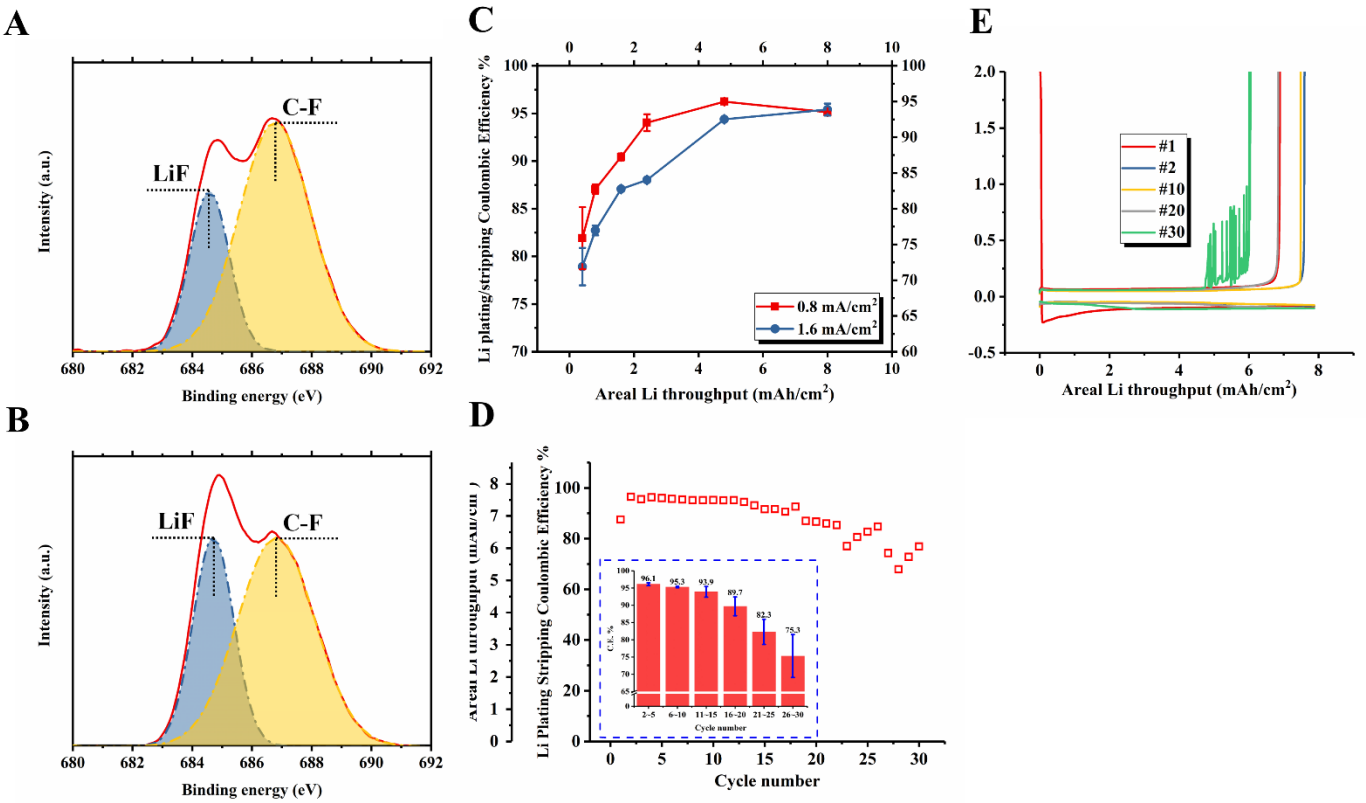

Figure 3. Li plating/stripping at planar and non-planar electrodes. XPS spectra of the surface layer formed on Li deposits harvested from: a) planar and (b) non-planar electrodes in 1M $LiPF_6$ EC/DMC electrolyte containing 10w% FEC. (c) Li plating/stripping Coulombic efficiencies on planar current collector at different areal Li throughputs in 1M $LiPF_6$ EC/DMC. (d) Li plating/stripping Coulombic efficiency and (e) corresponding voltage profile of planar current collector (Li throughput = 8 mAh/cm^2).

Lithium orphaning occurs when the metal becomes electronically disconnected from the current collector; while the ionic connection is maintained by contact with electrolyte. It has been extensively discussed in the literature as a failure mode for the Li anode but the role it plays in the poor reversibility of Li still lacks critical evaluation. Figure SI 5 illustrates how a non-planar electrode might prevent orphaning. Our results are consistent with this mechanism and imply that Li orphaning is both a substantial source of Li irreversibility and can be significantly suppressed, if not eliminated, when electronic access is sustained in a non-planar electrode that allows free expansion of the metal. In order to make these observations more concrete, we next attempt to isolate the effects of physical loss of Li by measuring the Li plating/stripping CE on Cu for different Li throughputs. To minimize the effect of chemical instability, we choose the 1M $LiPF_6$ EC/DMC-10%FEC electrolyte. Figs. 3A and 3B compare the interphases formed on Li in the planar Cu and non-planar electrode. It is seen that fluorinated species, including LiF, dominate the interphasial chemistry. The higher LiF fraction observed for the non-planar electrode is also consistent with the SEM observations in Fig 2 and SI 3, which show that the surface area of Li exposed to the electrolyte is higher for the non-planar case. Fig. 3C reports the CE at different

areal Li throughputs. Notably, the CE increases from 81.9% at 0.4 mAh/cm^2 to 96.2% at 4.8 mAh/cm^2 and 95.1% at 8.0 mAh/cm^2 (current density = 0.8 mA/cm^2), showing a strong initial dependence on throughput followed by a plateauing behavior. The initial rise in CE has to our knowledge not been reported but can be understood in a straightforward manner: chemical instability of Li is positively correlated to the exposed surface area. If Li forms a self-limiting, electrochemically inert SEI, the exposed surface area should be ideally invariant with increased Li throughput [19]. In other words, if a fixed amount of Li is consumed to form the SEI, the fraction of irreversible Li capacity associated with SEI formation should decrease approximately linearly with the Li throughput. This behavior is consistent with the initial rise observed but is not consistent with the plateau at higher Li throughputs.

The plateau implies that there is an interplay of multiple factors— e.g. the reduced chemical instability is offset by increasingly prominent Li orphaning at the higher Li throughputs. This explanation is supported by results reported in Figs. 3D & 3E where it is observed that after 10 high-CE plating/stripping cycles at 8 mAh/cm^2, the CE measured in Li||Cu cells becomes increasingly erratic (see magnitude of the error bars in the inset of Fig. 3D), and on average lower as cycling progresses. These behaviors are accompanied by strong and obvious fluctuations in the discharge voltage (Fig. 3E), particularly in the Li stripping segment of the cycle. They are quite different from what is observed at a lower Li throughput of 0.8 mAh/cm^2 (see SI 6) where neither the erratic CE nor the voltage fluctuations are observed in extended Li plate/strip cycling in the same electrolyte. They are also completely absent in cells that utilize a non-planar electrode (Fig. 1A-F), even at comparably high nominal Li throughputs (8 mAh/cm^2).

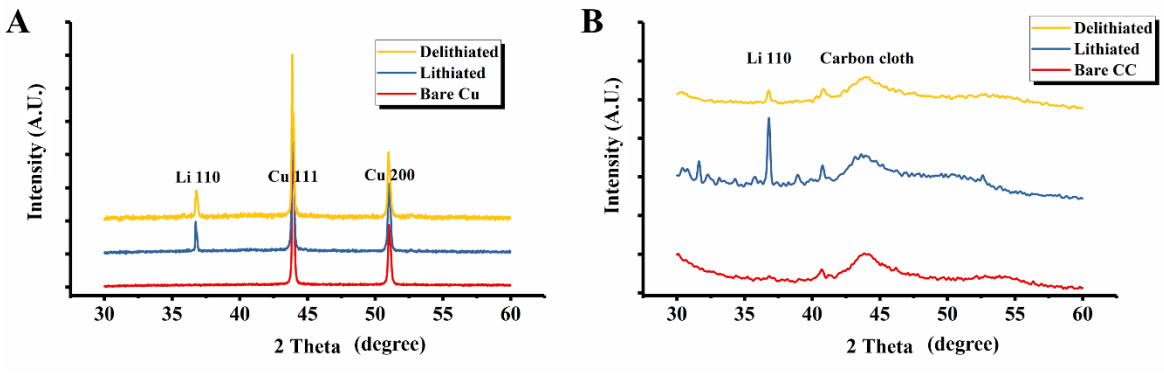

Figure 4. X-ray diffraction analysis of Li electrodeposits. XRD patterns of Li electrodeposits harvested after 30 cycles delithiated to 2 V from (A) planar and (B) non-planar electrodes.

We ascribe the erratic CE and voltage fluctuations to the possibility that orphaned Li in one plating/stripping cycle can be reconnected when Li is deposited appropriately in the following cycles. This random breakage and rebuilding of electronic access to Li (see scheme in SI 7) would lead to the observed scattering of the CE. Similarly, in the stripping cycle, orphaned Li can be reconnected due to morphological change, causing the potential spikes— the potential drops back to near 0 V v.s. Li+/Li when a piece of orphaned lithium is reconnected. Results reported in Fig. 4A confirm that orphaned Li is indeed responsible for the observed behaviors. Specifically, the figure reports x-ray diffraction (XRD) data for Li plated and stripped from Cu foil after 30 Li plating/stripping cycles (delithiated to 2V v.s. Li^+/Li). It is apparent from the figure that a strong Li 110 peak at 35.9° 2θ is observed on Cu even after the delithiation step, indicating that a large amount of electrochemically inactive Li remains stranded at the electrode. It is significant that none of these behaviors are present in any of the electrolytes studied when a non-planar electrode is used. Fig. 4B for instance shows that delithiation of Li leads to a nearly complete disappearance

of the Li 110 XRD peak. The non-planar electrode appears to prevent orphaning by maintaining continuous electrochemical access to the Li electrodeposit.

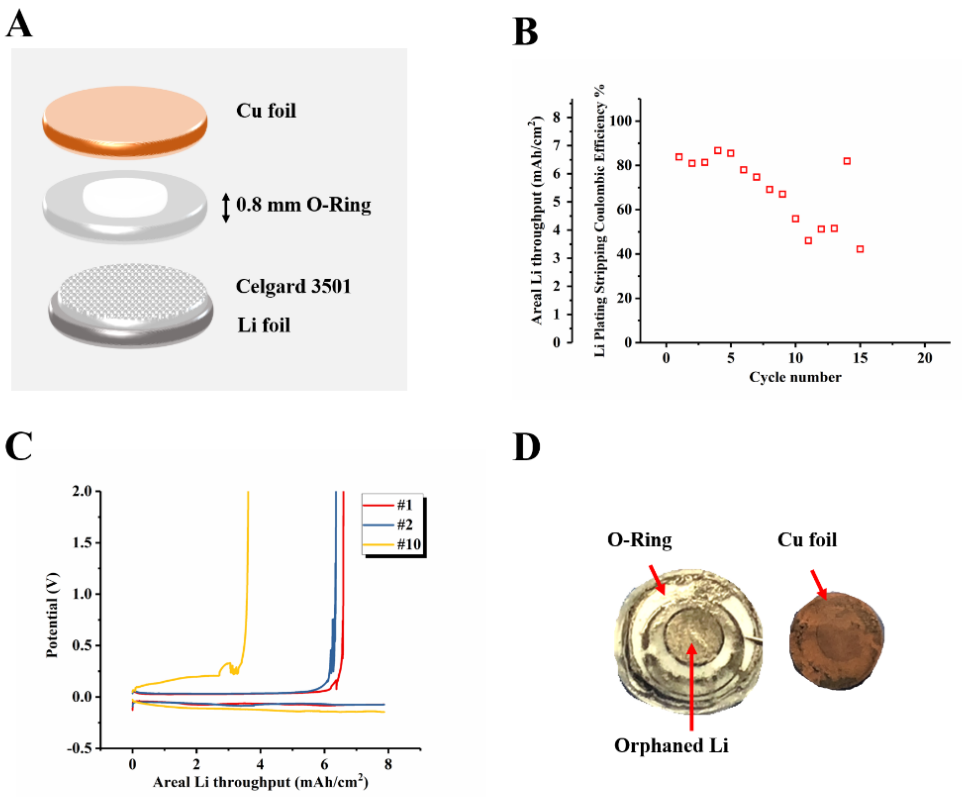

Figure 5. Li plating/stripping in pressure-free O-Ring separated coin cell. (a) schematic illustration of the O-Ring separated coin cell. (b) Li plating/stripping Coulombic efficiency and (c) corresponding voltage profile measured in the cell. (d) Photo showing orphaned Li detached from the planar Cu substrate filling the internal space of the O-Ring separator.

Furthermore, we removed the separator from the planar Li||Cu cells and evaluated the CE and morphology of Li electrodeposits. We designed an O-Ring separated coin cell (Fig. 5A) in which the backpressure produced by a conventional separator is removed. To avoid interference from dendrite-induced short circuits, a Celgard separator was placed between the O-Ring and the Li foil. Fig. 5B shows that the CE and reversibility are generally low (~80% for the initial 5 cycles, and <

50% thereafter). Fig. 5C reveals noticeable voltage spikes and fluctuations from the very first cycle. We opened the coin cells after 15 cycles (delithiated to 2 V v.s. Li^+/Li), and even from visual inspection it can be seen that the originally empty space in the O-Ring is filled with orphaned Li (Fig. 5D). SEM characterization (SI 8) shows that Li that remains in contact with Cu is essentially identical to that achieved in Li||Cu cells that use a separator or those that use a non-planar electrode. These findings indicate that physical loss of Li due to orphaning plays a rather large role in the poor reversibility of the Li metal anode. Our findings call attention to the need for more advanced non-planar anode architectures [27, 28] with nanoscale structure that are, for example, better matched to the length scales of Li electrodeposit fiber dimensions than the simple carbon-cloth material used in the present study. We expect such electrode designs will ensure more complete electronic access to orphaned Li and appear essential for progress towards highly reversible Li anodes.

As a final step, to further confirm the concept herein reported and to demonstrate its significance in battery applications, we assembled Li metal full cells will practical high areal capacity, i.e. 7~8 mAh/cm^2. Figure 6 reports the cycling performance of high areal capacity Li||$LiFePO_4$ full cells (N:P=1:1), in which 7 mAh/cm^2 Li deposited on carbon cloth serves as the anode. The high-loading cathode used in the study was fabricated using a non-planar architecture reported very recently [18] (See SI 9 for details). As we discussed in a recent publication [18], a practical N:P ratio for Li metal battery should be no larger than 5:1 to achieve an energy density that outperforms that of a battery using graphite anode; while the cyclability of a planar Li metal anode under such conditions is unsatisfactory.

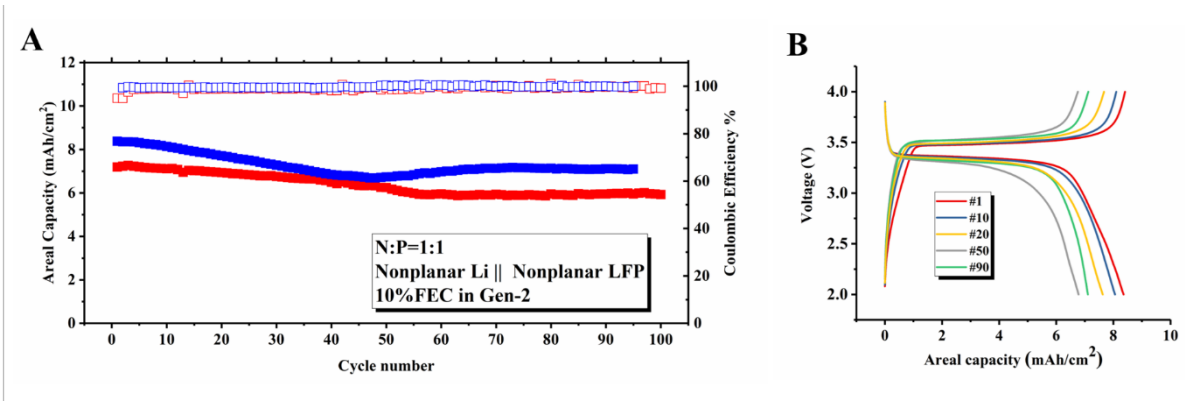

Figure 6. Performance of non-planar Li||LFP full cells. (a) Cycling performance (blue: 8 mAh/cm^2, red: 7 mAh/cm^2; N:P ≈ 1:1) in a 1M $LiPF_6$ EC/DMC electrolyte containing 10w% FEC (i.e. Gen-2 electrolyte). (b) Voltage profile of the 8 mAh/cm^2 full cell.

By contrast, as shown in Fig. 6A, when a nonplanar anode current collector is used, even with a stringent N:P=1:1 ratio (i.e 100% excess Li) and high areal Li throughputs, the Li||$LiFePO_4$ full cells claim 82.2% capacity retention after 100 cycles (7 mAh/cm^2 cell) and 84.6% capacity retention after 95 cycles (8 mAh/cm^2 cell, voltage profile in Fig. 6B). The capacity fading within the first ~50 cycles may be attributed to the gradual formation of interphasial species, e.g. SEI and cathode electrolyte interphase (CEI). If we ignore the initial rise in CE apparent in Figs. 1C and 1E, the results are consistent with a cell-level average $CE_{avg} = \exp\left(\frac{\ln\left[\frac{0.825}{2}\right]}{70}\right) * 100\% = 98.7\%$, which is close to the measured values. This means that nearly full capacity of both electrodes is achieved in our cycling study. Interestingly, after a gradual decrease, the capacity retention increases slightly at ~50 cycles and stabilizes. This phenomenon is tentatively attributed to the evolution of SEI into a more favorable one that facilitates fast kinetics, as indicated by the reduced overpotential shown in Fig. 1D inset and Fig. 6B. Our findings therefore show that a non-planar

anode significantly enhances the long-term reversibility of Li metal, and open up the avenue towards practical high energy density Li metal cells with stringent N:P ratio.

In conclusion, by interrogating the electrochemical properties and morphology of Li electrodeposits formed in a non-planar, carbon-cloth electrode in various liquid electrolytes, we find that relative to the more commonly studied chemical and morphological instabilities, physical orphaning of Li is the key cause of poor reversibility of Li metal anodes. With successful prevention of physical orphaning by building robust non-planar electronic pathways in the anode, we show further that Li anodes with high levels of reversibility can be created even when the metal electrodeposits in obviously dendritic morphologies. We also demonstrated Li metal full cells with stringent N:P=1:1 ratio that claim above 80% capacity retention over 100 cycles, which paves the way for practical Li metal batteries.

ACKNOWLEDGEMENTS

The research was supported as part of the Center for Mesoscale Transport Properties, an Energy Frontier Research Center supported by the U.S. Department of Energy (DOE), Office of Science, Basic Energy Sciences, under Award DE-SC0012673. The authors express their gratitude to Jiaqian Ma, Laijin Luo and Prof. Xiangzhong Ren for valuable discussions.

Supporting Information

The Supporting Information is available free of charge on the ACS Publications website at DOI: XXXXXX

Materials and methods, Schematic illustration of Li loss caused by dendritic electrodeposition, Measurement of intercalation capacity of carbon cloth, SEM of Lithium deposition morphology on planar current collector, Statistical analysis of fiber diameters of Li electrodeposits, Schematic illustration of guaranteed electronic pathways via nonplanar current collector, Li plating/stripping Coulombic efficiency and corresponding voltage profile of planar current collector, Schematic illustration of random reconnection of orphaned Li, SEM images of the orphaned Li in O-Ring separated coin cell, SEM and EDS mapping of nonplanar LFP electrode.

References

1. Lin, D.; Liu, Y.; Cui, Y., Reviving the lithium metal anode for high-energy batteries. Nature nanotechnology 2017, 12 (3), 194.
2. Albertus, P.; Babinec, S.; Litzelman, S.; Newman, A., Status and challenges in enabling the lithium metal electrode for high-energy and low-cost rechargeable batteries. Nature Energy 2017, 1.
3. Tikekar, M. D.; Choudhury, S.; Tu, Z.; Archer, L. A., Design principles for electrolytes and interfaces for stable lithium-metal batteries. Nature Energy 2016, 1 (9), 16114.
4. Kim, M. S.; Ryu, J.-H.; Lim, Y. R.; Nah, I. W.; Lee, K.-R.; Archer, L. A.; Cho, W. I., Langmuir–Blodgett artificial solid-electrolyte interphases for practical lithium metal batteries. Nature Energy 2018, 3 (10), 889.
5. Tu, Z.; Choudhury, S.; Zachman, M. J.; Wei, S.; Zhang, K.; Kourkoutis, L. F.; Archer, L. A., Designing artificial solid-electrolyte interphases for single-ion and high-efficiency transport in batteries. Joule 2017, 1 (2), 394-406.
6. Li, N. W.; Yin, Y. X.; Yang, C. P.; Guo, Y. G., An artificial solid electrolyte interphase layer for stable lithium metal anodes. Advanced materials 2016, 28 (9), 1853-1858.
7. Choudhury, S.; Archer, L. A., Lithium fluoride additives for stable cycling of lithium batteries at high current densities. Advanced Electronic Materials 2016, 2 (2), 1500246.
8. Suo, L.; Xue, W.; Gobet, M.; Greenbaum, S. G.; Wang, C.; Chen, Y.; Yang, W.; Li, Y.; Li, J., Fluorine-donating electrolytes enable highly reversible 5-V-class Li metal batteries. Proceedings of the National Academy of Sciences 2018, 115 (6), 1156-1161.
9. Qian, J.; Henderson, W. A.; Xu, W.; Bhattacharya, P.; Engelhard, M.; Borodin, O.; Zhang, J.-G., High rate and stable cycling of lithium metal anode. Nature communications 2015, 6, 6362.
10. Li, W.; Yao, H.; Yan, K.; Zheng, G.; Liang, Z.; Chiang, Y.-M.; Cui, Y., The synergetic effect of lithium polysulfide and lithium nitrate to prevent lithium dendrite growth. Nature communications 2015, 6, 7436.
11. Liu, S.; Xia, X.; Zhong, Y.; Deng, S.; Yao, Z.; Zhang, L.; Cheng, X. B.; Wang, X.; Zhang, Q.; Tu, J., 3D TiC/C Core/Shell Nanowire Skeleton for Dendrite-Free and Long-Life Lithium Metal Anode. Advanced Energy Materials 2018, 8 (8), 1702322.
12. Zhao, H.; Lei, D.; He, Y. B.; Yuan, Y.; Yun, Q.; Ni, B.; Lv, W.; Li, B.; Yang, Q. H.; Kang, F., Compact 3D Copper with Uniform Porous Structure Derived by Electrochemical Dealloying as Dendrite-Free Lithium Metal Anode Current Collector. Advanced Energy Materials 2018, 8 (19), 1800266.
13. Liang, Z.; Lin, D.; Zhao, J.; Lu, Z.; Liu, Y.; Liu, C.; Lu, Y.; Wang, H.; Yan, K.; Tao, X., Composite lithium metal anode by melt infusion of lithium into a 3D conducting scaffold with lithiophilic coating. Proceedings of the National Academy of Sciences 2016, 113 (11), 2862-2867.
14. Ye, H.; Zheng, Z. J.; Yao, H. R.; Liu, S. C.; Zuo, T. T.; Wu, X. W.; Yin, Y. X.; Li, N. W.; Gu, J. J.; Cao, F. F., Guiding Uniform Li Plating/Stripping through Lithium–Aluminum Alloying Medium for Long-Life Li Metal Batteries. Angewandte Chemie International Edition 2019, 58 (4), 1094-1099.
15. Ryou, M. H.; Lee, D. J.; Lee, J. N.; Lee, Y. M.; Park, J. K.; Choi, J. W., Excellent cycle life of lithium-metal anodes in lithium-ion batteries with mussel-inspired polydopamine-coated separators. Advanced Energy Materials 2012, 2 (6), 645-650.
16. Shin, W.-K.; Kannan, A. G.; Kim, D.-W., Effective suppression of dendritic lithium growth using an ultrathin coating of nitrogen and sulfur codoped graphene nanosheets on polymer separator for lithium metal batteries. ACS applied materials & interfaces 2015, 7 (42), 23700-23707.
17. Li, J.; Ma, C.; Chi, M.; Liang, C.; Dudney, N. J., Solid electrolyte: The key for high-voltage lithium batteries. Advanced Energy Materials 2015, 5 (4), 1401408.

18. Zheng, J.; Zhao, Q.; Liu, X.; Tang, T.; Bock, D. C.; Bruck, A. M.; Tallman, K. R.; Housel, L. M.; Kiss, A. M.; Marschilok, A. C., Nonplanar Electrode Architectures for Ultrahigh Areal Capacity Batteries. ACS Energy Letters 2018, 4 (1), 271-275.
19. Adams, B. D.; Zheng, J.; Ren, X.; Xu, W.; Zhang, J. G., Accurate determination of Coulombic efficiency for lithium metal anodes and lithium metal batteries. Advanced Energy Materials 2018, 8 (7), 1702097.
20. Geise, N. R.; Kasse, R. M.; Steinrueck, H.-G.; Toney, M. F. In Understanding Coulombic Efficiency Losses in Lithium Metal Anodes through Operando X-Ray Diffraction, Meeting Abstracts, The Electrochemical Society: 2018; pp 595-595.
21. Jiao, S.; Zheng, J.; Li, Q.; Li, X.; Engelhard, M. H.; Cao, R.; Zhang, J.-G.; Xu, W., Behavior of lithium metal anodes under various capacity utilization and high current density in lithium metal batteries. Joule 2018, 2 (1), 110-124.
22. Chen, S.; Niu, C.; Lee, H.; Li, Q.; Yu, L.; Xu, W.; Zhang, J.-G.; Dufek, E. J.; Whittingham, M. S.; Meng, S., Critical Parameters for Evaluating Coin Cells and Pouch Cells of Rechargeable Li-Metal Batteries. Joule 2019.
23. Steiger, J.; Kramer, D.; Mönig, R., Microscopic observations of the formation, growth and shrinkage of lithium moss during electrodeposition and dissolution. Electrochimica Acta 2014, 136, 529-536.
24. Chen, K.-H.; Wood, K. N.; Kazyak, E.; LePage, W. S.; Davis, A. L.; Sanchez, A. J.; Dasgupta, N. P., Dead lithium: mass transport effects on voltage, capacity, and failure of lithium metal anodes. Journal of Materials Chemistry A 2017, 5 (23), 11671-11681.
25. Brown, Z. L.; Jurng, S.; Nguyen, C. C.; Lucht, B. L., Effect of Fluoroethylene Carbonate Electrolytes on the Nanostructure of the Solid Electrolyte Interphase and Performance of Lithium Metal Anodes. ACS Applied Energy Materials 2018, 1 (7), 3057-3062.
26. Zhang, X. Q.; Cheng, X. B.; Chen, X.; Yan, C.; Zhang, Q., Fluoroethylene carbonate additives to render uniform Li deposits in lithium metal batteries. Advanced Functional Materials 2017, 27 (10), 1605989.
27. Guo, W.; Liu, S.; Guan, X.; Zhang, X.; Liu, X.; Luo, J., Mixed Ion and Electron-Conducting Scaffolds for High-Rate Lithium Metal Anodes. Advanced Energy Materials 2019, 1900193.
28. Wang, S. H.; Yin, Y. X.; Zuo, T. T.; Dong, W.; Li, J. Y.; Shi, J. L.; Zhang, C. H.; Li, N. W.; Li, C. J.; Guo, Y. G., Stable Li metal anodes via regulating lithium plating/stripping in vertically aligned microchannels. Advanced Materials 2017, 29 (40), 1703729.

TOC

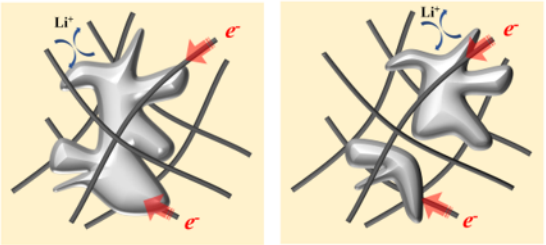

Is dendritic Li electrodeposition fatal?